Vertex Singularities Associated with Conical Points for the 3D Laplace Equation

T. Zaltzman,[1] **Z. Yosibash**[2]
[1] *Department of Engineering, Sapir College, Shaar Ha-Negev, Israel*

[2] *Department of Mechanical Engineering, Pearlstone Center for Aeronautical Engineering Studies, Ben-Gurion University of the Negev, Beer-Sheva 84105, Israel*

Received 15 March 2009; accepted 8 September 2009
Published online 6 November 2009 in Wiley Online Library (wileyonlinelibrary.com).
DOI 10.1002/num.20545

The solution u to the Laplace equation in the neighborhood of a vertex in a three-dimensional domain may be described by an asymptotic series in terms of spherical coordinates $u = \sum_i A_i \rho^{\nu_i} f_i(\theta, \varphi)$. For conical vertices, we derive explicit analytical expressions for the eigenpairs ν_i and $f_i(\theta, \varphi)$, which are required as benchmark solutions for the verification of numerical methods. Thereafter, we extend the modified Steklov eigen-formulation for the computation of vertex eigenpairs using p/spectral finite element methods and demonstrate its accuracy and high efficiency by comparing the numerically computed eigenpairs to the analytical ones. Vertices at the intersection of a crack front and a free surface are also considered and numerical eigenpairs are provided. The numerical examples demonstrate the efficiency, robustness, and high accuracy of the proposed method, hence its potential extension to elasticity problems. © 2009 Wiley Periodicals, Inc. Numer Methods Partial Differential Eq 27: 662–679, 2011

Keywords: Laplace equation; Steklov method; vertex singularities

I. INTRODUCTION

It is well known that solutions to the Laplace equation in the vicinity of a vertex in three-dimensional (3D) domains exhibit singularities. Investigation of such singularities is of interest in electromagnetic fields and magnetic recording, as well as in heat transfer problems, which may be described in realistic 3D domains by the Laplace equation. These solutions are also of major interest in the theory of elasticity, governed by second-order elliptic PDEs, whose characteristics are similar to the Laplace equation.

Although singular points in 2D domains have been extensively investigated, the vertex singularities in 3D domains received much scant attention because of their complexity. To the best of our knowledge, numerical methods for the investigation of vertex of conical notches, specifically

Correspondence to: Z. Yosibash, Department of Mechanical Engineering, Pearlstone Center for Aeronautical Engineering Studies, Ben-Gurion University of the Negev, Beer-Sheva 84105, Israel (e-mail: zohary@bgu.ac.il)
Contract grant sponsor: Israel Science Foundation; contract grant number: 750/07

the exponents of the singularity, were first introduced in [1]. Stephan and Whiteman [2] and Beagles and Whiteman [3] investigated analytically several vertices for the Laplace equation in 3D, mainly with homogeneous Dirichlet boundary conditions (BCs) and analyzed a finite element method (FEM) for the computation of eigenvalues by discretizing the Laplace-Beltrami equation (error estimates provided but no numerical results).

Analytical methods for the computation of the singularity exponents for homogeneous Dirichlet BCs are provided in [3] and in [4, p. 45–48] for axisymmetric cases. In [5] the Laplace equation in the vicinity of a conical point with Neumann BCs is also discussed, with a graph describing the behavior of the eigenvalues for different opening angles ω.

In this article, we extend the modified Steklov method, presented in [6] in the context of 2D problems, for the computation of eigenpairs associated with vertex singularities of the Laplace equation. We first provide analytical solutions for conical vertices for simplified problems in section II against which our numerical methods will be compared to demonstrate their convergence rate and accuracy. In section III, we formulate the weak eigenproblem, i.e., the modified Steklov formulation, and cast it in the form suitable for spectral/p finite element discretization. This method is aimed at computing the eigenpairs in a very efficient and accurate manner and may be generalized for multimaterial interfaces and elasticity operator. Numerical examples are considered in section IV—we first consider two problems for which analytical eigenpairs are provided in section II to demonstrate the accuracy and efficiency of the proposed numerical methods, followed by two more complicated example problems for which analytical results are unavailable.

II. ANALYTICAL SOLUTIONS FOR CONICAL VERTICES

Consider a 3D domain Ω having a rotationally symmetric conical vertex O on its boundary as shown in Fig. 1 with $\omega/2 \in [0, \pi]$. We aim at solving the Laplace equation with either homogeneous Dirichlet BCs in the vicinity of the conical point $\rho \to 0$:

$$\nabla^2 u(\rho, \theta, \varphi) = 0 \quad \text{in } \Omega, \tag{2.1}$$

$$u(\rho, \theta = \omega/2, \varphi) = 0 \quad \text{on } \partial\Omega_c, \tag{2.2}$$

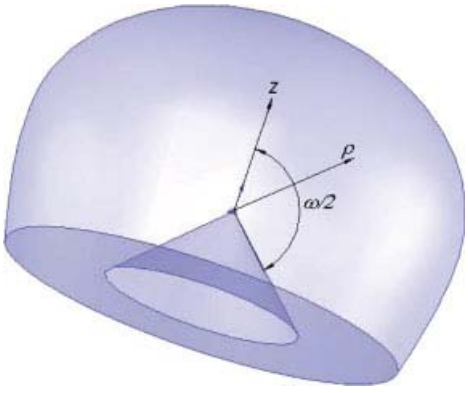

FIG. 1. Typical 3D domain with a rotationally symmetric conical vertex. [Color figure can be viewed in the online issue, which is available at wileyonlinelibrary.com.]

or with homogeneous Neumann BCs:

$$\frac{\partial u}{\partial n}(\rho,\theta=\omega/2,\varphi)=\frac{1}{\rho}\frac{\partial u(\rho,\theta=\omega/2,\varphi)}{\partial\theta}=0\quad\text{on }\partial\Omega_c, \tag{2.3}$$

where $\partial\Omega_c=\Gamma_c$ is the surface of the cone insert. Following [7], the solution is sought by separation of variables:

$$u(\rho,\theta,\varphi)=R(\rho)\Theta(\theta)\Phi(\varphi). \tag{2.4}$$

Substituting (2.4) in (2.1) one obtains a set of three ODEs as follows:

$$\rho^2R''+2\rho R'-\nu(\nu+1)R=0, \tag{2.5}$$

$$\Phi''+\mu^2\Phi=0, \tag{2.6}$$

$$-\sin^2(\theta)\Theta''-\sin(\theta)\cos(\theta)\Theta'-(\nu(\nu+1)\sin^2(\theta)-\mu^2)\Theta=0, \tag{2.7}$$

where $\nu(\nu+1)$ and μ^2 are separation constants. In (2.6) we chose the separation constant as μ^2 because it has to be positive if a periodic solution in φ is sought (for conical reentrant corners). The solution to (2.5) is of the form:

$$R(\rho)=A\rho^{\nu}, \tag{2.8}$$

where A is a generic constant. The restriction $\nu\geq 0$ has to hold true to obtain solutions that are in the Sobolev space $H^1(\Omega)$ (functions which have square zero and first derivatives integrable over the domain Ω, see [8]). The periodic solution to (2.6) is as follows:

$$\Phi=B\sin(\mu\varphi)+C\cos(\mu\varphi), \tag{2.9}$$

where B and C are generic constants. The periodicity constrain is $\Phi(\varphi)=\Phi(\varphi+2n\pi)$, therefore μ has to be a positive integer, i.e., $\mu=0,1,2,\ldots\overset{\text{def}}{=}m$. The case $m=0$ is associated with axisymmetric solutions, independent of φ.

Changing variables $z=\cos(\theta)$, the ODE (2.7) becomes:

$$(1-z^2)\frac{d^2\Theta}{dz^2}-2z\frac{d\Theta}{dz}+\left[\nu(\nu+1)-\frac{m^2}{1-z^2}\right]\Theta=0, \tag{2.10}$$

with homogeneous Dirichlet BCs:

$$\Theta(z_0)=0\quad\Rightarrow\quad\Theta(\cos\omega/2)=0, \tag{2.11}$$

or homogeneous Neumann BCs:

$$\frac{1}{\rho}\frac{d\Theta(z_0)}{d\theta}=0\quad\Rightarrow\quad\frac{d\Theta(\cos\omega/2)}{d\theta}=0. \tag{2.12}$$

z in general may be a complex variable, and m,ν are parameters that may take arbitrary real or complex values, called spherical harmonics.

The solution to (2.10) consists of a linear combination of first and second kind associated Legendre functions of degree ν and order m, denoted by $P_\nu^m(z)$ and $Q_\nu^m(z)$, respectively. That is,

$$\Theta(z)=DP_\nu^m(z)+EQ_\nu^m(z)\quad\Rightarrow\quad\Theta(\cos\theta)=DP_\nu^m(\cos\theta)+EQ_\nu^m(\cos\theta), \tag{2.13}$$

where D and E are generic constants. For $m = 0$ the Legendre functions of the second kind tend to ∞ along the axis of symmetry of the domain, hence we set $E \equiv 0$. Furthermore, for $m > 0$ the leading term of $Q_\nu^m(z)$ is as follows:

$$2^{m/2-1}\Gamma(m)\cos(m\pi)(1-z)^{-m/2},$$

then at $\theta = 0$, i.e., $z = 1$, $Q_\nu^m(\cos 0)$ is unbounded, thus one must choose $E = 0$, which reduces the solution (2.13) to:

$$\Theta(\cos\theta) = D P_\nu^m(\cos\theta), \tag{2.14}$$

where $P_\nu^m(\cos(\omega/2))$ is the associated Legendre function of the first kind. For example, for the case $m = 0$, the Legendre function P_ν can be computed using the Mehler-Dirichlet formula [7, (7.4.10)]:

$$P_\nu(\cos\omega/2) = \frac{\sqrt{2}}{\pi}\int_0^{\omega/2} \frac{\cos\left(\nu+\frac{1}{2}\right)t}{\sqrt{\cos t - \cos(\omega/2)}}dt. \tag{2.15}$$

It is important to notice that [7]

$$P_\nu^m(\cos\theta) = P_{-1-\nu}^m(\cos\theta), \tag{2.16}$$

which has the following important implication on the solution: if a given P_ν^m is a solution then so is $P_{-1-\nu}^m$, i.e., if a given ν is found to satisfy the BCs, so will $-1-\nu$.

Because there are an infinite number of νs that are determined by the BCs (detailed in the next subsection), each being a root of the Legendre function $P_{\nu_\ell}^m$, we denote them by two indices $\nu_\ell^{(m)}$, so the overall solution can be represented by:

$$u(\rho,\theta,\phi) = \sum_{m=0}\sum_{\ell=1} \rho^{\nu_\ell^{(m)}}\left[A_{m,\ell}\sin(m\varphi) + B_{m,\ell}\cos(m\varphi)\right]P_{\nu_\ell}^m(\cos\theta). \tag{2.17}$$

A. Homogeneous Dirichlet BCs

Consider for example the domain in Fig. 1 with the conical point at the apex of a cone insert having a solid angle $\omega = 6\pi/4$. There is an infinite number of νs for which the homogeneous Dirichlet BC (2.2) holds true. These νs are found by the root of (2.2):

$$P_\nu^m(\cos 3\pi/4) = 0, \tag{2.18}$$

m = 0 - Axisymmetric Solution. For the case $m = 0$ (2.18) reads $P_\nu(\cos 3\pi/4) = 0$. Using Mathematica [9] one may easily obtain the following first four non-negative $\nu^{(0)}$s for which (2.18) holds true:

$$\nu_1^{(0)} = 0.463098561780106, \quad \nu_2^{(0)} = 1.81322787311022$$
$$\nu_3^{(0)} = 3.153048711303707, \quad \nu_4^{(0)} = 4.48976080342872.$$

The associated Legendre functions of first kind are shown in Fig. 2.

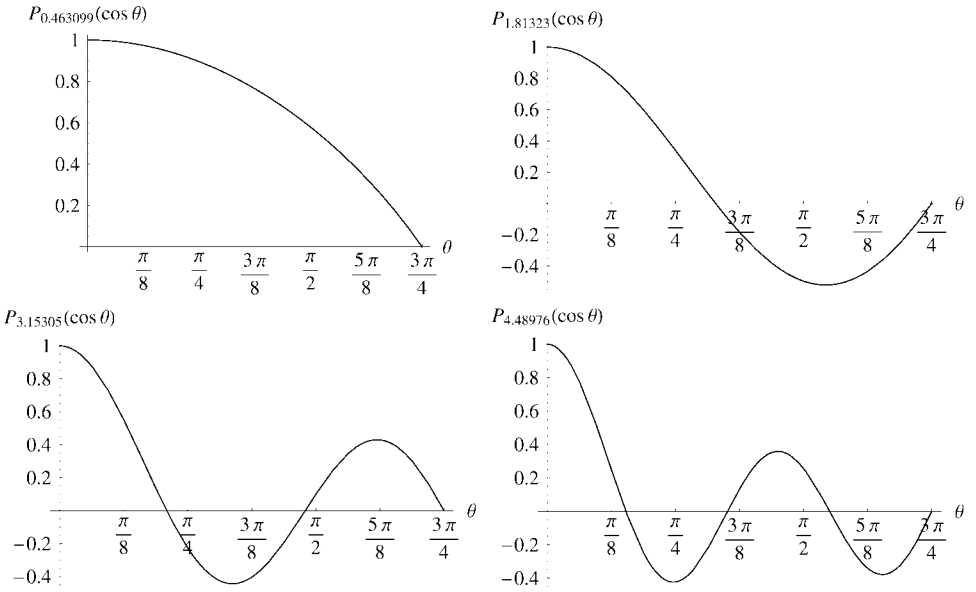

FIG. 2. First four eigenfunctions, Dirichlet BCs for conical point having a solid angle $3\pi/4$.

For each of the $\nu_i^{(0)}$s a solution of the form

$$u_i(\rho,\theta,\varphi) = A_i \rho^{\nu_i^{(0)}} P_{\nu_i^{(0)}}(\cos\theta)$$

is obtained, so that the overall solution is a linear combination:

$$u(\rho,\theta,\varphi) = \sum_i A_i \rho^{\nu_i^{(0)}} P_{\nu_i^{(0)}}(\cos\theta). \tag{2.19}$$

Remark 2.1. Notice that since $\nu_1^{(0)} < 1$ the first derivative is unbounded as $\rho \to 0$

***m* = 1, 2, 3, ...** For an arbitrary m the solution of $P_\nu^m(\cos 3\pi/4) = 0$ is obtained with 15 digits accuracy using the numerical algorithms within Mathematica [9]. We summarize in Table I the first four νs for $m = 0, 1, 2, 3$.

In Fig. 3 we plot the variation of the smallest eigenvalues $\nu_1^{(0)}$, $\nu_1^{(1)}$, and $\nu_1^{(2)}$ as a function of ω starting from a flat plate $\omega/2 = \pi/2$ till a reentrant line $\omega/2 = \pi$.

TABLE I. First four νs for $m = 0, 1, 2, 3$ for Dirichlet BC associated with $\omega = 6\pi/4$.

	$\nu_1^{(m)}$	$\nu_2^{(m)}$	$\nu_3^{(m)}$	$\nu_4^{(m)}$
$m = 0$	0.46309856178010	1.81322787311022	3.153048711303707	4.48976080342872
$m = 1$	1.24507709100149	2.54898557133218	3.868541068328044	5.19403335518201
$m = 2$	2.13656665895361	3.37380855301073	4.655359106556064	5.95715662710399
$m = 3$	3.07712950983885	4.25338593246190	5.492126885263152	6.76456426448560

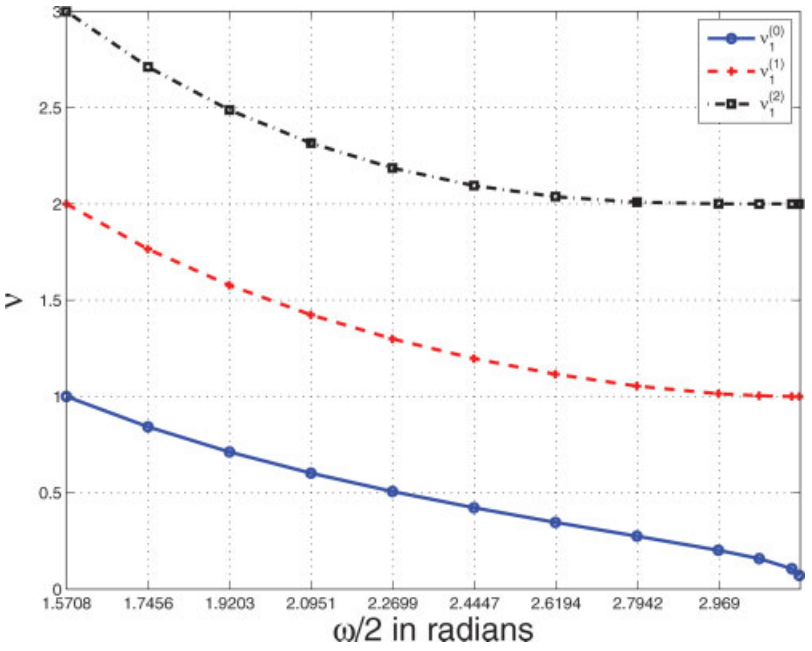

FIG. 3. $\nu_1^{(0)}$, $\nu_1^{(1)}$, and $\nu_1^{(2)}$, as a function of the cone reentrant angle ω, Dirichlet BCs. [Color figure can be viewed in the online issue, which is available at wileyonlinelibrary.com.]

B. Homogeneous Neumann BCs

For the same domain as in subsection A with $\omega = 6\pi/4$ the homogeneous Neumann BC (2.3) reads:

$$\frac{1}{\rho}\frac{dP_\nu^m(\cos\theta)}{d\theta}\bigg|_{\theta=3\pi/4} = 0 \quad \Rightarrow \quad -\sin\theta\frac{dP_\nu^m(\cos\theta)}{d\cos\theta}\bigg|_{\theta=3\pi/4} = 0. \tag{2.20}$$

By using the recursive formula [7, (7.12.16) on p. 195]:

$$\left(z^2-1\right)\frac{dP_\nu^m(z)}{dz} = \nu z P_\nu^m(z) - (\nu+m)P_{\nu-1}^m(z), \tag{2.21}$$

the BC (2.20) becomes:

$$\cos(3\pi/4)\nu P_\nu^m(\cos 3\pi/4) - (\nu+m)P_{\nu-1}^m(\cos 3\pi/4) = 0, \tag{2.22}$$

for which an infinite number of νs exists.

The smallest non-negative eigenvalue is 0, associated with the so-called rigid body motion (known to exist for homogeneous Neumann BCs) and is of no interest as it describes a constant solution.

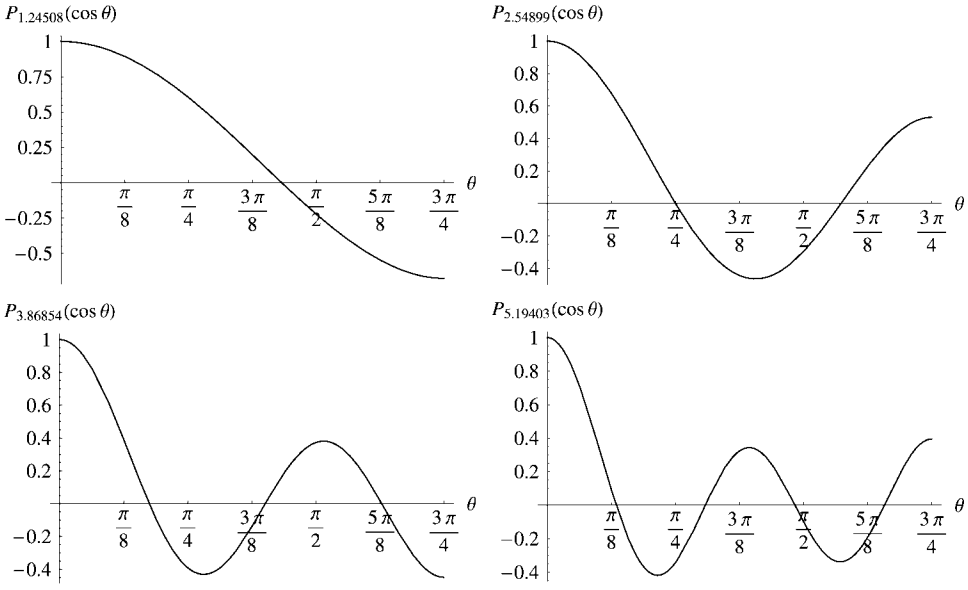

FIG. 4. First four eigenfunctions associated with $m = 0$, Neumann BCs, $\omega = 6\pi/4$.

Axisymmetric Solution. The first four non-negative (and nonzero) νs for $m = 0$ for which (2.22) holds true are as follows:

$$\nu_1^{(0)} = 1.24507709100149, \quad \nu_2^{(0)} = 2.548985521168983$$
$$\nu_3^{(0)} = 3.86854093155942, \quad \nu_4^{(0)} = 5.194033355182022$$

The associated Legendre eigenfunctions of the first kind are shown in Fig. 4.
For an arbitrary m we summarize in Table II the first four (nonzero) νs for $m = 0, 1, 2, 3$.

III. THE MODIFIED STEKLOV WEAK FORM AND FINITE ELEMENT DISCRETIZATION

Herein, we develop the formulation and numerical procedures that will efficiently and reliably compute approximations for the singular solutions (eigenpairs) for such problems when used in conjunction with the spectral/p-version of the FEM. The proposed method, named the "modified Steklov method" [6, 10], is in general, applicable to singularities associated with corners, nonisotropic multimaterial interfaces and abrupt changes in BCs.

TABLE II. First four νs for $m = 0, 1, 2, 3$ for Newmann BC associated with $\omega = 6\pi/4$.

	$\nu_1^{(m)}$	$\nu_2^{(m)}$	$\nu_3^{(m)}$	$\nu_4^{(m)}$
$m = 0$	1.2450770910	2.54898552117	3.86854093156	5.19403335518
$m = 1$	0.8571676765	2.00000000000	3.27090467124	4.57561722130
$m = 2$[a]	1.8742536963	2.88678057132	4.08498821549	5.35319993628
$m = 3$[b]	2.9130094418	3.84636536605	4.96120003163	6.18222599268

[a]For $m = 2$, $\nu = 1$ is also an eigensolution, but $P_1^2(\cos\theta) \equiv 0$.
[b]For $m = 3$, $\nu = 1, 2$ are also eigensolutions, but $P_1^3(\cos\theta) = P_2^3(\cos\theta) \equiv 0$.

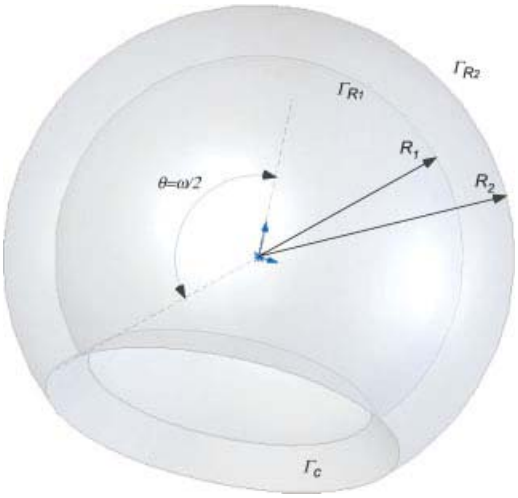

FIG. 5. The subdomain Ω_R in the vicinity of the vertex. [Color figure can be viewed in the online issue, which is available at wileyonlinelibrary.com.]

Consider (2.1–2.2) or (2.3) in the vicinity of the vertex, in an artificial subdomain Ω_R created by the intersection of Ω with two spheres of radii $R_1 < R_2$ as shown in Fig. 5. As the solution in the vicinity of the vertex is of the form $u = \rho^\nu f(\theta, \varphi)$ on the surface of the sphere R_1 one obtains:

$$\frac{\partial u}{\partial n}(\rho = R_1) = -\frac{\partial u}{\partial \rho}(\rho = R_1) = -\nu R_1^{\nu-1} f(\theta, \varphi) = -\frac{\nu}{R_1} u(R_1, \theta, \varphi). \tag{3.1}$$

Similarly, on the surface of the sphere R_2, one obtains:

$$\frac{\partial u}{\partial n}(\rho = R_2) = \frac{\partial u}{\partial \rho}(\rho = R_2) = \frac{\nu}{R_2} u(R_2, \theta, \varphi). \tag{3.2}$$

Thus, the strong (classical) modified Steklov formulation in Ω_R (see [6]) is obtained:

$$\nabla^2 u(\rho, \theta, \varphi) = 0 \quad \text{in } \Omega_R \tag{3.3}$$

$$\frac{1}{\rho} \frac{\partial u(\rho, \theta = \omega/2, \varphi)}{\partial \theta} = 0 \quad \text{or} \quad u(\rho, \theta = \omega/2, \varphi) = 0 \quad \text{on } \Gamma_c \stackrel{\text{def}}{=} \partial\Omega_c, \tag{3.4}$$

$$\frac{\partial u}{\partial n}(\rho = R_1) = -\frac{\nu}{R_1} u(R_1, \theta, \varphi) \quad \text{on } \Gamma_{R_1}, \tag{3.5}$$

$$\frac{\partial u}{\partial n}(\rho = R_2) = \frac{\nu}{R_2} u(R_2, \theta, \varphi) \quad \text{on } \Gamma_{R_2}. \tag{3.6}$$

The strong modified Steklov formulation may be brought to a weak form by multiplying (3.3) by a test function $v(\rho, \theta, \varphi)$ integrating over Ω_R and using Green's theorem to obtain:

$$\iiint_{\Omega_R} (\nabla u) \cdot (\nabla v) d\Omega = \iint_{\partial\Omega_R} \frac{\partial u}{\partial n} v dS \tag{3.7}$$

For homogeneous Neumann or Dirichlet BCs on $\partial\Omega_c$ that part of the boundary diminishes in the RHS of (3.7), and considering (3.5)–(3.6) one finally obtains the weak modified Steklov eigen-formulation:

$$\begin{gathered}\text{Seek } \nu \in \Re \text{ and } 0 \neq u \in \mathcal{E}(\Omega_R) \text{ such that } \forall v \in \mathcal{E}(\Omega_R) \\ \mathcal{B}(u,v) = \nu\big(\mathcal{M}_{R_2}(u,v) - \mathcal{M}_{R_1}(u,v)\big),\end{gathered} \tag{3.8}$$

where

$$\mathcal{B}(u,v) \overset{\text{def}}{=} \int_{\rho=R_1}^{R_2}\int_{\theta=0}^{\frac{\omega}{2}}\int_{\varphi=0}^{2\pi}\left(\rho^2\sin\theta\frac{\partial u}{\partial\rho}\frac{\partial v}{\partial\rho} + \sin\theta\frac{\partial u}{\partial\theta}\frac{\partial v}{\partial\theta} + \frac{1}{\sin\theta}\frac{\partial u}{\partial\varphi}\frac{\partial v}{\partial\varphi}\right)d\rho\, d\theta\, d\varphi, \tag{3.9}$$

$$\begin{aligned}\nu\big(\mathcal{M}_{R_2}(u,v) - \mathcal{M}_{R_1}(u,v)\big) \overset{\text{def}}{=} \nu\Bigg(& R_2\int_{\theta=0}^{\frac{\omega}{2}}\int_{\varphi=0}^{2\pi} u\; v\big|_{R_2}\sin\theta\, d\theta\, d\varphi \\ & - R_1\int_{\theta=0}^{\frac{\omega}{2}}\int_{\varphi=0}^{2\pi} u\; v\big|_{R_1}\sin\theta\, d\theta\, d\varphi\Bigg).\end{aligned} \tag{3.10}$$

Here, $\mathcal{E}(\Omega_R)$ denotes the energy space, containing of all functions which have finite square first derivatives integrable over the domain Ω_R, see [8].

Remark 3.1. Notice that in 2D [6] the RHS of the weak form is independent of the radius of the circular domain, whereas in 3D there is an explicit dependency on R_1 and R_2.

Remark 3.2. For homogeneous Dirichlet BCs, the energy space $\mathcal{E}(\Omega_R)$ is restricted to functions that automatically satisfy these (see also [6] for the space $\overset{\circ}{\mathcal{E}}(\Omega_R)$).

Remark 3.3. The third term in the integrand in (3.9) is singular due to the term $\frac{1}{\sin\theta}$. A remedy for this difficulty may be obtained if a nonsymmetric weak formulation is considered.

Remark 3.4. The weak formulation (3.8) may be generalized to cases that involve a V-notch or a crack front (see e.g., Figs. 8–10). In these cases, the integral on the variable φ is to be performed from 0 to φ_2 (the solid angle of the V-notch opening – a crack is a V-notch for which $\varphi_2 = 2\pi$). We generalize the formulation for these latter cases in the following.

A. A Nonsymmetric Weak Eigenform

In view of remark 3.3, we multiply (3.3) by a special test function $\sin\theta w(\rho,\theta,\varphi)$ and follow the steps described earlier to obtain a nonsymmetrical weak modified Steklov eigen-formulation that does not contain singular terms:

$$\begin{gathered}\text{Seek } \nu \in \Re \text{ and } 0 \neq u \in \mathcal{E}(\Omega_R), \text{ such that } \forall w \in \mathcal{E}(\Omega_R) \\ \tilde{\mathcal{B}}(u,w) = \nu\big(\tilde{\mathcal{M}}_{R_2}(u,w) - \tilde{\mathcal{M}}_{R_1}(u,w)\big),\end{gathered} \tag{3.11}$$

where

$$\tilde{\mathcal{B}}(u,w) \stackrel{\text{def}}{=} \int_{\rho=R_1}^{R_2}\int_{\theta=0}^{\frac{\omega}{2}}\int_{\varphi=0}^{\varphi_2}\Big(\rho^2\sin^2\theta\frac{\partial u}{\partial\rho}\frac{\partial w}{\partial\rho}+\sin^2\theta\frac{\partial u}{\partial\theta}\frac{\partial w}{\partial\theta} + \frac{\partial u}{\partial\varphi}\frac{\partial w}{\partial\varphi}+\frac{\sin(2\theta)}{2}\frac{\partial u}{\partial\theta}w\Big)d\rho\,d\theta\,d\varphi, \quad (3.12)$$

$$\nu\big(\tilde{\mathcal{M}}_{R_2}(u,v)-\tilde{\mathcal{M}}_{R_1}(u,v)\big) \stackrel{\text{def}}{=} \nu\Big(R_2\int_{\theta=0}^{\frac{\omega}{2}}\int_{\varphi=0}^{\varphi_2} u\,w\big|_{R_2}\sin^2\theta\,d\theta\,d\varphi - R_1\int_{\theta=0}^{\frac{\omega}{2}}\int_{\varphi=0}^{\varphi_2} u\,w\big|_{R_1}\sin^2\theta\,d\theta\,d\varphi\Big). \quad (3.13)$$

For convenience of numerical application (and for future use of the p-FE method), we perform a change of variables in (3.12–3.13) as follows:

$$\rho=\frac{1-\xi}{2}R_1+\frac{1+\xi}{2}R_1 \quad\rightarrow\quad d\rho=\frac{R_2-R_1}{2}d\xi, \quad (3.14)$$

$$\theta=\frac{1+\eta}{2}\frac{\omega}{2} \quad\rightarrow\quad d\theta=\frac{\omega}{4}d\eta, \quad (3.15)$$

$$\varphi=\frac{1+\zeta}{2}\varphi_2 \quad\rightarrow\quad d\varphi=\frac{\varphi_2}{2}d\zeta, \quad (3.16)$$

so that (3.12–3.13) become:

$$\begin{aligned}\tilde{\mathcal{B}}(u,w) &= \frac{\omega\varphi_2}{4(R_2-R_1)}\iiint_{-1}^{1}\rho^2(\xi)\sin^2\theta(\eta)\frac{\partial u}{\partial\xi}\frac{\partial w}{\partial\xi}\,d\xi\,d\eta\,d\zeta,\\ &+\frac{(R_2-R_1)\varphi_2}{\omega}\iiint_{-1}^{1}\sin^2\theta(\eta)\frac{\partial u}{\partial\eta}\frac{\partial w}{\partial\eta}\,d\xi\,d\eta\,d\zeta,\\ &+\frac{(R_2-R_1)}{4}\Big(\frac{\omega}{\varphi_2}\iiint_{-1}^{1}\frac{\partial u}{\partial\zeta}\frac{\partial w}{\partial\zeta}\,d\xi\,d\eta\,d\zeta\\ &\qquad+\varphi_2\iiint_{-1}^{1}\frac{\sin(2\theta(\eta))}{2}\frac{\partial u}{\partial\eta}w\,d\xi\,d\eta\,d\zeta\Big), \end{aligned} \quad (3.17)$$

$$\nu\big(\tilde{\mathcal{M}}_{R_2}(u,v)-\tilde{\mathcal{M}}_{R_1}(u,v)\big) = \nu\frac{\omega\varphi_2}{8}\Big[\iint_{-1}^{1}\big(R_2(u\,w)\big|_{\xi=1}-R_1(u\,w)\big|_{\xi=-1}\big)\sin^2\theta(\eta)\,d\eta\,d\zeta\Big]. \quad (3.18)$$

Application of p/Spectral Finite Element Methods. The weak form (3.11) may be represented in terms of a matrix formulation using the p-version or spectral FEM. The finite dimensional space corresponding to the weak form is spanned by a set of shape functions $N_i(\xi,\eta,\zeta)$, $i=1,\ldots,(p+1)(q+1)(s+1)$, where $(p+1)$ represents the number of basis

functions that span the functional space in ξ ($(q+1)$, $(s+1)$ correspond to the number of basis functions in η and ζ correspondingly). In terms of the shape functions and their coefficients, one has $u = \sum_{i=1}^{(p+1)(q+1)(s+1)} a_i N_i(\xi,\eta,\zeta) = \vec{a}_{\text{tot}}^T \vec{N}$ and similarly $v = w = \vec{N}^T \vec{b}_{\text{tot}}$. Denoting by $\vec{a}_R$ and $\vec{b}_R$ the coefficients that multiply basis functions that are nonzero on Γ_{R_1} and Γ_{R_2}, (3.8) or (3.11) becomes:

$$[K]\vec{a}_{\text{tot}} = \nu \begin{bmatrix} [M_{R_1}] & [0] \\ [0] & [M_{R_2}] \end{bmatrix} \vec{a}_R, \tag{3.19}$$

where $[K]$ is the stiffness matrix, and $[M_{R_i}]$ are the generalized mass matrices corresponding to the terms in $\vec{a}_R$ on the boundaries Γ_{R_i}.

We may partition $\vec{a}_{\text{tot}} = \{\vec{a}_R,\ \vec{a}_{\text{in}}\}$. By partitioning $[K]$, we may represent the eigenproblem (3.19) in the form:

$$\begin{bmatrix} [K_R] & [K_{R-\text{in}}] \\ [K_{\text{in}} - R] & [K_{\text{in}}] \end{bmatrix} \{\vec{a}_R\ ,\ \vec{a}_{\text{in}}\} = \nu \begin{bmatrix} [M_{R_1}] & [0] \\ [0] & [M_{R_2}] \end{bmatrix} \vec{a}_R. \tag{3.20}$$

The relation in (3.20) can be used for eliminating $\vec{a}_{\text{in}}$ by using static condensation, thus obtaining the reduced eigenproblem:

$$[K_S]\vec{a}_R = \nu \begin{bmatrix} [M_{R_1}] & [0] \\ [0] & [M_{R_2}] \end{bmatrix} \vec{a}_R, \tag{3.21}$$

where:

$$[K_S] = [K_R] - [K_{R-\text{in}}][K_{\text{in}}]^{-1}[K_{\text{in}-R}].$$

For the solution of (3.21), it is important to note that $[K_S]$ is, in general, a full matrix. However, as the order of the matrices is relatively small, the solution is inexpensive.

Remark 3.5. For conical vertices the solution in Ω_R is regular and the p/spectral FEM will converge exponentially [11], and furthermore also the dual eigenpairs are obtained as solutions of the form $\rho^{-\nu-1} \in \mathcal{E}(\Omega_R)$.

Remark 3.6. Homogeneous Dirichlet BCs on one or more of the boundaries are applied in the numerical algorithm according to [12]. We substitute 0s in the rows and columns corresponding to unknown values on the boundaries in the matrices $[K]$, $[M_{R_i}]$, except the diagonal terms which is set equal to 1 in $[K]$ and a small value, let us call it b, in $[M_{R_i}]$. This procedure is equivalent to restricting the space in which the functions belong to $\overset{\circ}{\mathcal{E}}(\Omega_R)$. If we perform this procedure on n rows, for example, we obtain n "artificial eigenvalues" equal to $1/b$. In our numerical examples, we chose $b = 0.01$ to produce very large "artificial eigenvalues" all equal to 100.

The Basis Functions. We construct the basis functions so that the first $2(q+1)(s+1)$ are nonzero on the two boundaries $\rho = R_1$ and $\rho = R_2$, whereas all the other are zero on these two boundaries. A polynomial basis (in terms of the variable $-1 \le t \le 1$, based on the Legendre

polynomials [11]) is chosen to represent the solution in $\rho(\xi)$, $\theta(\eta)$, or $\varphi(\zeta)$ (t is replaced by ξ or η or ζ):

$$
\begin{aligned}
P_1(t) &= (1-t)/2,\\
P_2(t) &= (1+t)/2,\\
P_3(t) &= \sqrt{\frac{3}{8}}(t^2-1),\\
P_4(t) &= \sqrt{\frac{5}{8}}t(t^2-1),\\
P_5(t) &= \sqrt{\frac{7}{128}}(5t^4-6t^2+1),\\
P_6(t) &= \sqrt{\frac{9}{128}}t(7t^4-10t^2+3),\\
P_7(t) &= \sqrt{\frac{11}{512}}(21t^6-35t^4+15t^2-1),\\
P_8(t) &= \sqrt{\frac{13}{512}}t(33t^6-63t^4+35t^2-5),\\
P_9(t) &= \sqrt{\frac{15}{32768}}(429t^8-924t^6+630t^4-140t^2+5).
\end{aligned}
$$

If the domain of interest has a conical vertex as shown in Fig. 1, the basis functions have to be periodic in φ with a period of 2π. Therefore, in this case, a sin and cos basis are chosen as the basis functions in φ:

$$
Q_k(\zeta) = \begin{cases} \cos(k\frac{1+\zeta}{4}\varphi_2) & k = 0,2,4,6,\ldots \\ \sin((k+1)\frac{1+\zeta}{4}\varphi_2) & k = 1,3,5,7,\ldots \end{cases}. \tag{3.22}
$$

Otherwise, for nonperiodical solutions as the vertices in the domains shown in Figs. 8 and 10, the polynomial basis is chosen to represent the solution in φ variable.

Therefore, the basis functions are defined as:

$$
N_{i+(s+1)(j-1)+(s+1)(q+1)(k-1)}(\xi,\eta,\zeta) = \begin{cases} P_i(\xi)P_j(\eta)Q_k(\zeta) & \text{Periodical solutions} \\ P_i(\xi)P_j(\eta)P_k(\zeta) & \text{Nonperiodical solutions} \end{cases}
$$
$$
i = 1,\ldots,p+1, \quad j = 1,\ldots,q+1, \quad k = 1,\ldots,s+1, \tag{3.23}
$$

resulting in a $(p+1)(q+1)(s+1)\times(p+1)(q+1)(s+1)$ stiffness matrix $[K]$ which after static condensation is reduced to a $2(q+1)(s+1)\times 2(q+1)(s+1)$ eigenproblem. The formulation described herein was implemented using the Mathematica package [9] for the generation of the required matrices and the computation of the eigenvalues and eigenvectors.

TABLE III. Conical point with $\omega/2 = 3\pi/4$ and homogeneous Neumann BCs.

p,q,s DOFs	1,1,1 8 DOFs	1,2,2 18 DOFs	1,4,4 50 DOFs	1,6,6 98 DOFs	1,8,8 162 DOFs	2,8,8 243 DOFs
$\nu_1^{(1)} = 0.85716767$	0.83175 (−2.96%)	0.85812 (0.11%)	0.85728 (1.3E−2%)	0.857172 (1.0E−3%)	0.857169 (1.5E−4%)	0.857168 (4.0E−5%)
$\nu_1^{(0)} = 1.24507709$	1.21102 (−2.73%)		1.25547 (8.3E−1%)	1.24441 (−5.4E−2%)	1.24503 (−3.8E−3%)	1.24503 (−3.8E−3%)
$\nu_1^{(2)} = 1.87425369$			1.87508 (4.4E−2%)	1.87439 (7.0E−3%)	1.87438 (6.7E−3%)	1.87425 (−2E−4%)
$\nu_2^{(1)} = 2.00000000$	2.09971 (4.99%)	2.0664 (3.32%)	2.00036 (1.8E−2%)	2.00018 (9.0E−3%)	2.00018 (9.0E−3%)	2.000001 (5E−5%)
$\nu_2^{(0)} = 2.54898552$		2.72871 (7.05%)	2.57948 (1.19%)	2.54832 (−2.6E−2%)	2.54971 (2.8E−2%)	2.54915 (6.4E−3%)
$\nu_2^{(2)} = 2.88678057$			2.89257 (2.0E−1%)	2.88773 (3.3E−2%)	2.88774 (3.3E−2%)	2.88678 (−2E−5%)
$\nu_1^{(3)} = 2.91300944$				2.914 (3.4E−2%)	2.91401 (3.4E−2%)	2.91301 (2E−5%)

Convergence of first seven e-values (except first e-value, which is 0) for $R_1 = 0.95$ as the approximation functional space is enriched.
In parenthesis the relative error in % is reported.

IV. NUMERICAL EXAMPLES

Four example problems are considered. The first two correspond to a conical vertex with either homogeneous Neumann or homogeneous Dirichlet BCs for which analytical solutions are available, so that the convergence rate of the modified Steklov nonsymmetric method can be assessed. The third example problem is a vertex generated at the intersection of a crack front and a flat plane with homogeneous Neumann BCs. This case is considered because the artificial subdomain contains a singular edge (along the crack front), therefore the convergence rate is slower. This example problem does not have an analytical solution and numerical approximations are provided. The last example problem corresponds to a vertex at the intersection of a V-notch front with a conical reentrant corner, with homogeneous Neumann BCs where a singular edge also exists in the subdomain along the V-notch front.

A. Conical Vertex, $\omega/2 = 3\pi/4$, Homogeneous Neumann BCs

We demonstrate the accuracy and efficiency of the modified Steklov nonsymmetric eigenformulation by considering a conical vertex with $\omega/2 = 3\pi/4$. We chose $R_1 = 0.95$ and $R_2 = 1$ because the eigenvalues are insensitive to R_1 (keeping $R_2 = 1$) for $R_1 > 0.9$. This is because the exact solution is in the form ρ^ν, which may be well represented by polynomials for $0.9 < \rho < 1$ (see also the 2D case in [6]). We first consider homogeneous Neumann BCs on Γ_c and summarize the first seven computed eigenvalues in Table III, together with the relative error in % defined as:

$$\text{Relative error } \% = \frac{100(\nu_i^{\text{FE}} - \nu_i^{\text{EX}})}{\nu_i^{\text{EX}}}$$

To better demonstrate the accuracy and fast convergence rate of the modified nonsymmetric Steklov method, we plot in Fig. 6 the relative error in percentage of the first five eigenvalues as the number of DOFs is increased. A clear high rate of convergence for the first eigenvalues is

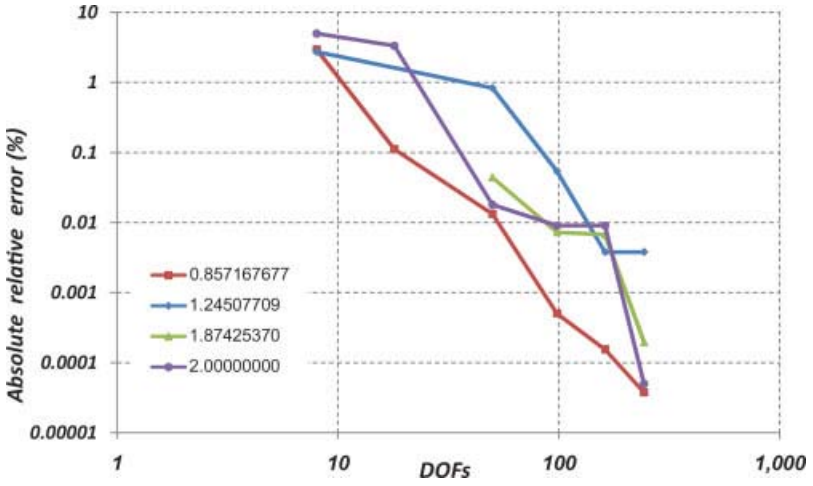

FIG. 6. Convergence of the first four nonzero eigenvalues ν for the conical vertex with $\omega/2 = 3\pi/4$ and homogeneous Neumann BCs. [Color figure can be viewed in the online issue, which is available at wileyonlinelibrary.com.]

observed, obtaining an accuracy of an order of $10^{-4}\%$ relative error with less than 300 DOFs but only 200 DOFs in the condensed eigenproblem.

B. Conical Vertex, $\omega/2 = 3\pi/4$, Homogeneous Dirichlet BCs

In this section, we consider the previous conical vertex with $\omega/2 = 3\pi/4$, $R_1 = 0.95$ and $R_2 = 1$ but homogeneous Dirichlet BCs are applied on Γ_c. The first five computed eigenvalues are summarized in Table IV, together with the relative error. The convergence rate of the first four eigenvalues is shown in the plot in Fig. 7. One may observe the fast rate of convergence in this example problem also.

TABLE IV. Conical point with $\omega/2 = 3\pi/4$ and homogeneous Dirichlet BCs.

p,q,s DOFs	1,2,2 18 DOFs	1,3,3 32 DOFs	1,4,4 50 DOFs	1,6,6 98 DOFs	1,8,8 162 DOFs
$\nu_1^{(0)} = 0.463098562$	0.483284 (4.4E0%)	0.452786 (−2.2E0%)	0.46808 (1.1E0%)	0.463774 (1.5E−1%)	0.463204 (2.3E−2%)
$\nu_1^{(1)} = 1.24507709$	1.24489 (−1.5E−2%)	1.24374 (−1.1E−1%)	1.2453 (1.8E−2%)	1.24509 (1.0E−3%)	1.24508 (2.3E−4%)
$\nu_2^{(0)} = 1.813227873$		1.69437 (−6.6E0%)	1.87592 (3.5E0%)	1.8105 (−1.5E−1%)	1.81333 (5.6E−3%)
$\nu_1^{(2)} = 2.136566659$			2.13683 (1.2E−2%)	2.13683 (1.2E−2%)	2.13681 (1.1E−2%)
$\nu_2^{(1)} = 2.54551186$	2.97811 (1.7E1%)	2.55054 (2.0E−1%)	2.55029 (1.9E−1%)	2.54961 (1.6E−1%)	2.54954 (1.6E−1%)

Convergence of first five e-values for $R_1 = 0.95$ as the approximation functional space is enriched.
In parenthesis the relative error in % is reported.

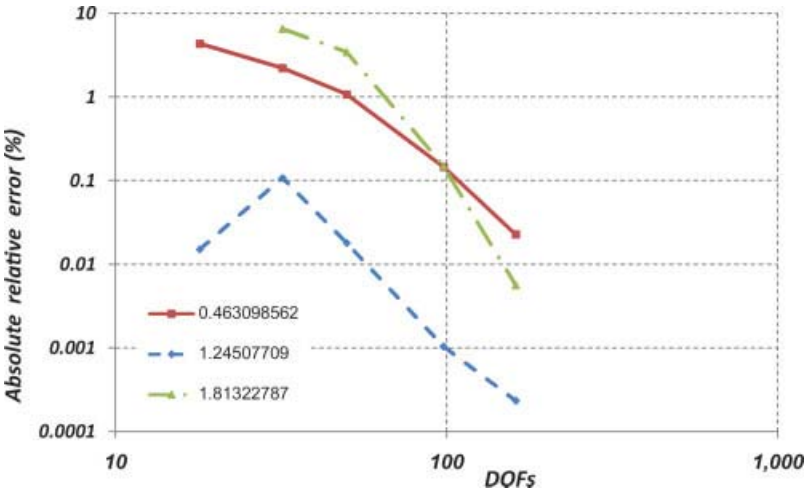

FIG. 7. Convergence of the first four nonzero eigenvalues ν for the conical vertex with $\omega/2 = 3\pi/4$ and homogeneous Dirichlet BCs. [Color figure can be viewed in the online issue, which is available at wileyonlinelibrary.com.]

C. Vertex at the Intersection of a Crack Front with a Flat Face, Homogeneous Neumann BCs

In many practical applications, cracks are present in 3D domains, and a vertex singularity exists at the intersection of the crack face with the boundary of the domain. Such a situation is described in Fig. 8, where a crack front intersects a flat free face. Homogeneous Neumann BCs are prescribed on the crack surfaces and the flat face.

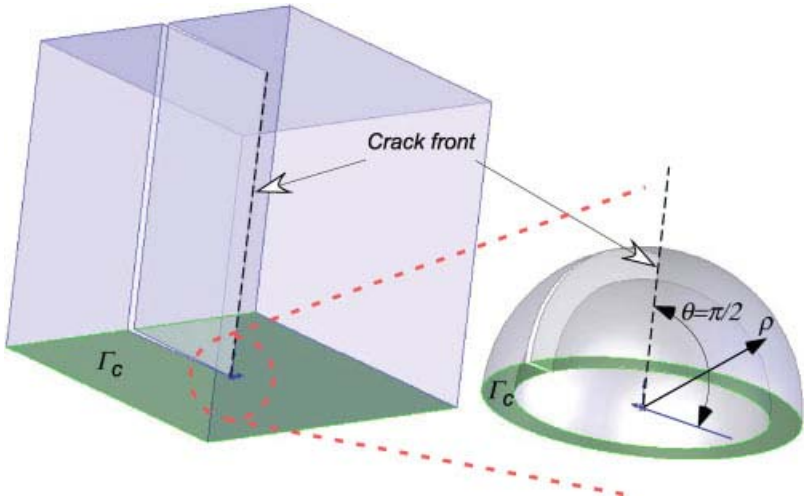

FIG. 8. A crack front intersecting a free face. Right: The 3D domain with the crack. Left: The artificial subdomain used for the computation of the eigenpairs. [Color figure can be viewed in the online issue, which is available at wileyonlinelibrary.com.]

TABLE V. Vertex at the intersection of a crack front with a free face.

p,q,s DOFs	1,1,1 8 DOFs	2,3,3 48 DOFs	2,4,4 75 DOFs	2,6,6 147 DOFs	2,9,9 300 DOFs
$\nu_{Est} = 0.5$	0.47575 (−4.8E0%)	0.4855969 (−2.9E0%)	0.4906311 (−1.9E0%)	0.4950594 (−9.9E−1%)	0.4975721 (−4.9E−1%)
$\nu_{Est} = 1.0$		1.2325059 (2.3E1%)	1.0036215 (3.6E−1%)	1.0000167 (1.7E−1%)	1.0000000 (2.5E−6%)
$\nu_{Est} = 1.5$				1.4950602 (−3.3E−1%)	1.5000010 (6.9E−5%)
$\nu_{Est} = 2.0$	2.31019 (1.6E1%)	2.0759202 (3.8E0%)	2.0308122 (1.5E0%)	1.9992894 (−3.6E−2%)	1.9999832 (−8.4E−4%)

Convergence of first five e-values (except first e-value, which is 0) for $R_1 = 0.95$ as the approximation functional space is enriched.

Taking $R_1 = 0.95$ and $R_2 = 1$, we summarize the first five, computed eigenvalues in Table V. For this example problem, the analytical eigenvalues are unknown, but estimated to be 0, 0.5, 1, 1.5 and 2.0, and the relative error is computed relative to the estimated values.

The convergence rate of the first four eigenvalues is shown in the plot in Fig. 9. Because the computational domain contains a singular edge, along the crack front, the convergence of the first (most singular) eigenvalue is much slower compared to the previous two example problems. A remedy to this situation is the use of a p-FE method, and refine the computational mesh in the vicinity of the singular edge. However, this necessitates an assembly procedure, which is beyond the scope of this work. Nevertheless, high accuracy is achieved with the presented method with a moderate number of degrees of freedom.

D. Vertex at the Intersection of a V-Notch Front with a Conical Reentrant Corner, Homogeneous Neumann BCs

The last example problem is the vertex at the intersection of a conical insert with a reentrant corner as described in Fig. 10. Homogeneous Neumann BCs are prescribed on all surfaces and the flat face.

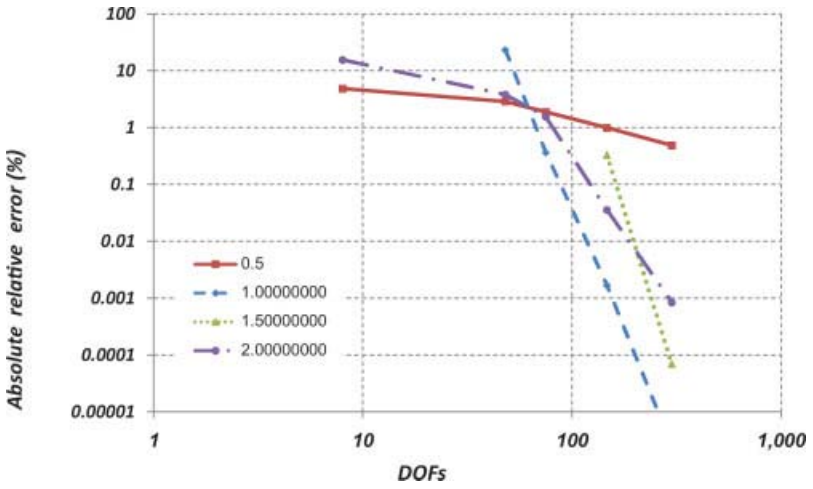

FIG. 9. Convergence of the first five nonzero eigenvalues ν for the crack front with a free face. [Color figure can be viewed in the online issue, which is available at wileyonlinelibrary.com.]

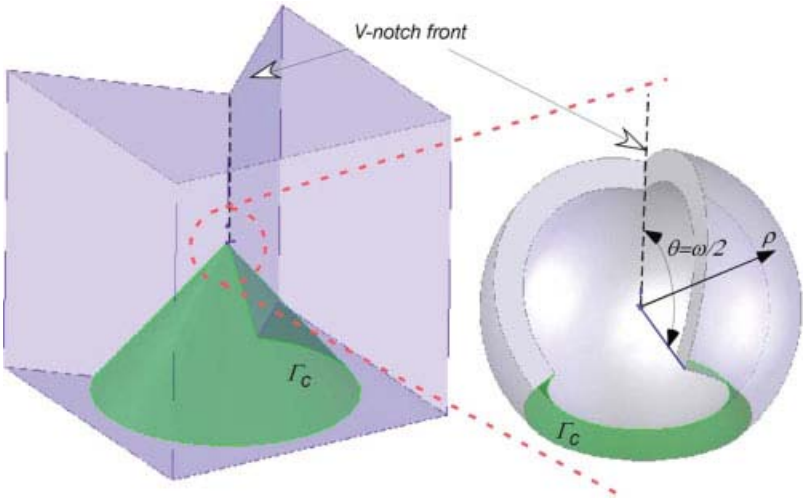

FIG. 10. A V-notch intersecting a conical reentrant corner. Right: The 3D domain. Left: The artificial subdomain used for the computation of the eigenpairs. [Color figure can be viewed in the online issue, which is available at wileyonlinelibrary.com.]

Taking $R_1 = 0.95$ and $R_2 = 1$, we summarize the first four (nonzero) computed eigenvalues in Table VI (first eigenvalue is zero so is not considered). For this example problem, the analytical eigenvalues are unknown, thus the relative error cannot be computed. One may easily noticed the clear convergence of the eigenvalues as the number of DOFs is increased.

Remark 4.1. In all four considered example problems, for each positive eigenvalue computed ν_i, the modified Steklov problem provided the negative eigenvalue $-1-\nu_i$ with high accuracy. This eigenvalue with the corresponding eigenfunction will be used in future studies for the extraction of the vertex stress-intensity-factor.

V. SUMMARY AND CONCLUSIONS

The modified Steklov method was extended herein for the computation of the eigenpairs associated with vertex singularities of the Laplace equation. It was brought to a nonsymmetric form to overcome integrand singularity and implemented in the context of a spectral method. Four

TABLE VI. Vertex at the intersection of a V-notch front with a conical reentrant corner, homogeneous Neumann BCs, $\omega/2 = 3\pi/4$, $\varphi_2 = 6\pi/4$.

$p,q,s = 1,2,2$ 18 DOFs	$p,q,s = 1,4,4$ 50 DOFs	$p,q,s = 1,6,6$ 98 DOFs	$p,q,s = 1,8,8$ 162 DOFs
0.600442	0.535591	0.536327	0.536642
1.068311	1.195313	1.19021	1.190185
1.503901	1.255467	1.24441	1.245032
1.741498	1.730020	1.72647	1.727616

Convergence of first four e-values (except first e-value, which is 0) for $R_1 = 0.95$ as the approximation functional space is enriched.

example problems were solved using the numerical method, and the results were compared to analytically derived eigenvalues so as to demonstrate its efficiency and accuracy. The generality of the method and the accurate results encourage the extension of this method to elasticity problems and multimaterial interfaces. For these cases, a p-FE method is necessary where the domain is partitioned into several elements, and an assembly procedure is required. Future research on the application of p-FEMs based on the modified Steklov formulation for the elasticity system is underway and will be reported in a future publication.

References

1. Z. P. Bažant and L. M. Keer, Singularities of elastic stresses and of harmonic functions at conical notches or inclusions, Int J Solids Struct 10 (1974), 957–964.
2. E. Stephan and J. R. Whiteman, Singularities of the Laplacian at corners and edges of three-dimensional domains and their treatment with finite element methods, Math Methods Appl Sci 10 (1988), 339–350.
3. A. E. Beagles and J. R. Whiteman, General conical singularities in three-dimensional Poisson problems, Math Methods Appl Sci 11 (1989), 215–235.
4. C. Bernardi, M. Dauge, and I. Maday, Spectral methods for axisymmetric domains, Gauthier-Villars - NH, Paris, France, 1999.
5. M. Dauge and M. Pogu, Existence et regularite de la fonction potentiel pour des ecoulements subcritiques s'etablissant autour d'un corps a singularite conique, Ann Faculte Sci Toulouse 9 (1988), 213–242.
6. Z. Yosibash and B. A. Szabó, Numerical analysis of singularities in two-dimensions. Part 1: Computation of eigenpairs, Int J Numer Methods Eng 38 (1995), 2055–2082.
7. N. N. Lebedev, Special functions and their applications, Prentice-Hall, Englewood Cliffs, NJ, USA, 1965.
8. C. Susanne Brenner and L. Ridgway Scott, The mathematical theory of finite element methods, Springer-Verlag, Berlin, 1994.
9. S. Wolfram, Mathematica5, Wolfram Research, USA, 2004.
10. I. Babuška, T. Von-Petersdorff, and B. Andersson, Numerical treatment of vertex singularities and intensity factors for mixed boundary value problems for the Laplace equation in R^3, SIAM J Numer Anal 31 (1994), 1265–1288.
11. B. A. Szabó and I. Babuška, Finite element analysis, Wiley, New York, 1991.
12. H. R. Schwartz, Finite element methods, Academic Press, London, UK, 1978.